Neutrinos from stellar collapse: Effects of flavor mixing

Gautam Dutta, D. Indumathi, M. V. N. Murthy, and G. Rajasekaran
The Institute of Mathematical Sciences, Chennai 600 113, India
(Received 22 July 1999; published 10 December 1999)

We study the effect of nonvanishing masses and mixings among neutrino flavors on the detection of neutrinos from stellar collapse by a water Cherenkov detector. We consider a realistic framework in which there are three neutrino flavors whose mass squared differences and mixings are constrained by the present understanding of solar and atmospheric neutrinos. We also include the effects of high dense matter within the supernova core. We find that the number of events due to the dominant process involving electron antineutrinos may change dramatically for some allowed mixing parameters. Furthermore, contributions from charged-current scattering off oxygen atoms in the detector can be considerably enhanced due to flavor mixing; such events have a distinct experimental signature since they are backward peaked.

PACS number(s): 14.60.Pq, 13.15.+g, 97.60.Bw

I. INTRODUCTION

The sighting of a supernova, SN 1987a in the Large Magellanic cloud (LMC) [1], led to great excitement, since, for the first time, the neutrinos from stellar collapse were detected by Earth-based detectors [2,3]. Unlike electromagnetic radiation, which takes a long time to emerge from the collapsing core, neutrinos provide direct information about core collapse. The direct observation of neutrinos from SN1987a by the Kamiokande (KII) [2] and the IMB [3] detectors forms the beginning of a new phase in neutrino astrophysics with far-reaching implications for particle physics. Since then, the KII detector has been upgraded with tremendous improvement both in size and resolution, and many new detectors such as SNO and Borexino will begin taking data soon.

Immediately after SN1987a, several authors analyzed [4–10] the neutrino events recorded by the KII and the IMB detectors. While the number of events was not statistically significant enough to obtain quantitative information on the neutrino spectrum, there was qualitative agreement between the predictions from the core collapse mechanism and the observations. The present situation with improved neutrino detectors affords a quantitative analysis of the neutrino events if a supernova collapse were to take place in the near future. While the observational scenario is positive, there has also been much progress in understanding the properties of neutrinos, namely, their masses and mixings, through analyses of solar and atmospheric neutrino puzzles [11]. Both the solar and atmospheric neutrino deficits that are observed conclusively point to the requirement of (at least) three neutrino generations and mixing among them. The masses and mixings are then constrained by the observed deficit in the neutrino fluxes [12,13].

In this paper, we analyze in detail the signatures of neutrinos from stellar collapse. The analysis is confined to type II supernovas (which occur when the initial mass of the star is between 8 and 20 solar masses) since the neutrino emission from these is significant enough to make reasonable predictions. We consider the emission of all three types of neutrino (and antineutrino) flavors. There exist many models of stellar collapse. The present understanding of neutrino emission involves dividing the neutrino emission into two distinct phases—the neutronization burst and thermal neutrino emission. The number of neutrinos emitted during the burst phase is only a few percent of the neutrinos emitted during the thermal or cooling phase of the protoneutron star. While only ν_e is emitted during the earlier phase, neutrinos and antineutrinos of all types are emitted during the final phase. Much of the binding energy of the neutron star is radiated away as neutrinos while a small fraction (a few percent or less) is deposited in the shock wave that blows away the mantle [14]. Detailed predictions for the luminosity and average energy as a function of time are available [15] for neutrinos emitted during the burst and cooling phases. We use these predictions as an input in our analysis.

An important fact to note is that the neutrinos, which are produced in the high-density region of the core, interact with matter before emerging from the supernova. The presence of nonzero masses and mixing in vacuum among various neutrino flavors results in strong matter-dependent effects, including conversion from one flavor to another. Hence, the observed neutrino flux in the detectors may be dramatically different for certain neutrino flavors, for certain values of the mixing parameters, due to neutrino oscillations. The effect of mixing on the neutrino signal from supernovas was analyzed in detail before by several authors [16–18]. The effect of masses and mixing on time-of-flight information has been discussed in [19,20].

Our analysis is based on the pioneering work of Kuo and Pantaleone [16] where they include mixing among all three neutrino flavors. However, unlike all previous analyses, we take into account the constraints on the neutrino mixing and masses imposed [12,13] by solutions consistent with the solar and atmospheric neutrino puzzles. There are several possible solutions here, including a purely vacuum solution for the solar neutrino problem. We choose some typical (allowed) values for the mixing angles, to illustrate the possible effects of mixing. This is important from the point of view of integrating known constraints on the neutrino masses and mixings in order to obtain a realistic picture of neutrino emissions from supernovas. We analyze in detail the dependence of the recoil energy spectra on the mixing parameters, at water Cherenkov detectors. In Sec. II we review the the-

oretical framework of our calculation, including a reanalysis of the matter effects on the neutrino spectrum in the hot dense core. Section III highlights the various inputs—neutrino fluxes and cross sections in the detector—that we have used in order to compute the event rate expected at water Cherenkov neutrino detectors. The numerical computation of the total number of events for the time-integrated neutrino spectrum and the effects of neutrino oscillation are discussed in Sec. IV, where the results are discussed and summarized. Some well-known results, adapted to the present situation, are discussed in Appendixes A and B for completeness.

II. THREE FLAVOR OSCILLATIONS IN HIGH DENSE MATTER

In this section, we discuss the mixing among three flavors of neutrinos (or antineutrinos) and compute the electron (or antielectron) neutrino survival probability P_{ee} (or $\overline{P}_{ee}$). We will explicitly show that these are the only relevant probabilities. While the theoretical details of this mixing are well known, the effects of superdense matter, such as is found in the stellar cores, are nontrivial. We shall also use this analysis to set our notation.

The three flavor eigenstates are related to the three mass eigenstates in vacuum through a unitary transformation

$$\begin{bmatrix} \nu_e \\ \nu_\mu \\ \nu_\tau \end{bmatrix} = U^v \begin{bmatrix} \nu_1 \\ \nu_2 \\ \nu_3 \end{bmatrix}, \tag{1}$$

where the superscript v on the right-hand side (RHS) stands for vacuum. The 3×3 unitary matrix U^v can be parametrized by three Euler angles (ω,ϕ,ψ) and a phase. The form of the unitary matrix can therefore be written, in general, as

$$U^v = U_{23}(\psi)\times U_{phase}\times U_{13}(\phi)\times U_{12}(\omega),$$

where $U_{ij}(\theta_{ij})$ is the mixing matrix between the ith and jth mass eigenstates with the mixing angle θ_{ij}. It has been shown that the expression for electron neutrino survival probability, integrated over the time of emission and of absorption, is independent of the phase and the third Euler angle ψ [21,22]. They can be set to zero without loss of generality and we have the following form for U^v :

$$U^v = \begin{pmatrix} c_\phi c_\omega & c_\phi s_\omega & s_\phi \\ -s_\omega & c_\omega & 0 \\ -s_\phi c_\omega & -s_\phi s_\omega & c_\phi \end{pmatrix}, \tag{2}$$

where $s_\phi = \sin\phi$ and $c_\phi = \cos\phi$, etc. The angles ω and ϕ can take values between 0 and $\pi/2$. Recently, the CHOOZ Collaboration set a laboratory limit on $\overline{\nu}_e$ oscillations [27] that resulted in a strong limit, $\phi<12°$, on the (13) mixing angle [28]. However, a combination of solar and atmospheric neutrino data allows for both large- and small-angle solutions for the (12) mixing angle ω. The angle ψ is large, typically of the order of $\psi\sim45°$ (although this is not relevant here). These constraints will be imposed later on in our numerical analysis.

The masses of the eigenstates in vacuum are taken to be μ_1, μ_2, and μ_3. In the mass eigenbasis, the $(\text{mass})^2$ matrix is diagonal:

$$\begin{aligned} M_0^2 &= \begin{pmatrix} \mu_1^2 & 0 & 0 \\ 0 & \mu_2^2 & 0 \\ 0 & 0 & \mu_3^2 \end{pmatrix} \\ &= \mu_1^2 II + \begin{pmatrix} 0 & 0 & 0 \\ 0 & \delta_{21} & 0 \\ 0 & 0 & \delta_{31} \end{pmatrix}, \\ &= \mu_1^2 II + \Delta M_0^2, \end{aligned} \tag{3}$$

where the mass-squared differences are given by $\delta_{21}=\mu_2^2-\mu_1^2$ and $\delta_{31}=\mu_3^2-\mu_1^2$. Without loss of generality, we can take δ_{21} and δ_{31} to be greater than zero; this defines the standard hierarchy of masses. Neutrino oscillation amplitudes are independent of the first term, so we drop it from further calculation. In the flavor basis, therefore, the relevant part of the mass-squared matrix has the form

$$\begin{aligned} \Delta M_v^2 &= U^v\,\Delta M_0^2\,U^{v\dagger} \\ &= \delta_{31}M_{31} + \delta_{21}M_{21}, \end{aligned} \tag{4}$$

where

$$M_{31} = \begin{pmatrix} s_\phi^2 & 0 & s_\phi c_\phi; \\ 0 & 0 & 0 \\ s_\phi c_\phi & 0 & c_\phi^2 \end{pmatrix},$$

$$M_{21} = \begin{pmatrix} c_\phi^2 s_\omega^2 & c_\phi s_\omega c_\omega & -c_\phi s_\phi s_\omega^2 \\ c_\phi s_\omega c_\omega & c_\omega^2 & -s_\phi s_\omega c_\omega \\ -c_\phi s_\phi s_\omega^2 & -s_\phi s_\omega c_\omega & s_\phi^2 s_\omega^2 \end{pmatrix}. \tag{5}$$

The relevant matter effects may be included by a modified mass-squared matrix,

$$\Delta M_m^2 = \delta_{31}M_{31} + \delta_{21}M_{21} + A(r)M_A, \tag{6}$$

where

$$M_A = \begin{pmatrix} 1 & 0 & 0 \\ 0 & 0 & 0 \\ 0 & 0 & 0 \end{pmatrix} \tag{7}$$

and $A(r)$ is given by

$$A(r) = \sqrt{2} G_F N_e(r) \times 2E, \tag{8}$$

which is proportional to the electron number density $N_e(r)$ in the supernova core. Here r is the radial distance from the center of the star. The detailed modifications due to matter effects are discussed in Appendix A.

The maximum value of A occurs at the core and is approximately $2\times10^7 E$ eV^2, where E is the neutrino energy in MeV. The modification due to the matter dependence is similar to the case of solar neutrinos, although, unlike in the case of solar neutrinos, all flavors are produced in the supernova core.

It is clear that the mass-squared matrix is no longer diagonal in the presence of matter; we therefore diagonalize ΔM_m^2 in order to determine the matter-corrected eigenstates. This is a difficult problem in general for arbitrary values of δ_{31} and δ_{21}. These are, however, constrained by the limits on them given by the simultaneous analysis of solar and atmospheric neutrino problems, namely, $10^{-3} \leqslant \delta_{31} \leqslant 10^{-2}$ eV^2 and $\delta_{21} < 10^{-4}$ eV^2, so that $\delta_{31} \sim \delta_{32}$; the value of A for energetic neutrinos (of a few MeV to tens of MeV) in the core is therefore several orders of magnitude greater than these mass-squared differences. The eigenvalue problem may thus be solved perturbatively, with the following hierarchy: $A(\text{core}) \gg \delta_{31} \gg \delta_{21}$. As a result, the electron neutrino undergoes two well-separated resonances when the value of $A(r)$ approaches the two mass-squared differences. Following Kuo and Pantaleone [16], and using the above mass hierarchy, the matter mixing angle ϕ_m is given by (see Appendix A for more details)

$$\tan 2\phi_m = \frac{\delta_{31} \sin 2\phi}{\delta_{31} \cos 2\phi - A}. \tag{9}$$

At the point of production inside the core, $A(\text{core}) \gg \delta_{31}$; thus, $\phi_m \to \pi/2$. This makes further calculations extremely simple, since the electron neutrino is produced as a pure $|\nu_3\rangle$ mass eigenstate in the core of the supernova. The survival probability of the electron neutrino is simply given by the projection of the $|\nu_3\rangle$ mass eigenstate onto the $|\nu_e\rangle$ flavor state in the detector, after correcting for the Landau-Zener jumps which may occur in the stellar matter during propagation. The average survival probability of the electron neutrino is therefore given by

$$\begin{aligned} P_{ee} &= \sum_{i,j=1}^{3} |U_{ei}^{v}|^2 |U_{ej}^{m}|^2 |\langle \nu_i^v | \nu_j^m \rangle|^2 \\ &= \sin^2\phi P_3 + \cos^2\phi \sin^2\omega P_2 + \cos^2\phi \cos^2\omega P_1 . \end{aligned} \tag{10}$$

Here ϕ and ω are the vacuum mixing angles defined earlier and P_i denote the Landau-Zener jump probabilities among the mass eigenstates,

$$P_1 = P_h P_l, \tag{11}$$

$$P_2 = P_h (1 - P_l), \tag{12}$$

$$P_3 = (1 - P_h), \tag{13}$$

where P_h and P_l denote the jump probabilities at the higher and at the lower resonances. In Appendix B we show that for the parameters values relevant in the case of neutrinos produced in the supernova core, P_h is actually very close to zero. Therefore to a good approximation, we may write

$$P_{ee} = \sin^2\phi. \tag{14}$$

This result implies that the propagation of neutrinos is adiabatic in the high-density core. We will support this conclusion in Appendix B. The information given above is not enough to obtain completely the survival and oscillation probabilities of the individual flavors. However, since the detectors we are interested in do not separately detect ν_μ and ν_τ, this is sufficient for our analysis. We shall therefore use this form for the survival probability for the numerical results calculated in the next section.

We now consider the case of $\overline{\nu_e}$ propagation in high-density matter. The only change in this case is that the matter-dependent term in the relevant part of the mass-squared matrix has the opposite sign [to that in Eq. (8)], that is,

$$A(r) = -\sqrt{2} G_F N_e(r) \times 2E. \tag{15}$$

The analysis goes through as in the case of ν_e propagation through matter and the mixing angle ϕ for antineutrinos in matter is given by

$$\tan 2\phi_m = \frac{\delta_{31} \sin 2\phi}{\delta_{31} \cos 2\phi + |A|}. \tag{16}$$

On using the fact that $A(\text{core}) \gg \delta_{31}$, we obtain $\phi_m \to 0$ in contrast to the solution $\phi_m \to \pi/2$ for electron neutrinos. Thus $\overline{\nu_e}$ is produced in the mass eigenstate, $|\overline{\nu_1}\rangle$, in the core of the supernova. There are no Landau-Zener jumps to consider in this case since the resonance conditions are never satisfied unless the mass hierarchy is altered. The propagation is therefore adiabatic and the survival probability is obtained by simply projecting the $|\overline{\nu_1}\rangle$ eigenstate onto the flavor eigenstate in vacuum (at the detector). The antineutrino survival probability is therefore given by

$$\overline{P}_{ee} = \cos^2\phi \cos^2\omega, \tag{17}$$

where ϕ and ω are as usual the vacuum mixing angles defined earlier.

III. NEUTRINO FLUXES AND CROSS SECTIONS

We need the inputs of neutrino flux emission at the supernova and the neutrino cross section at the detector in order to obtain the event rates. We begin with a discussion of the neutrino fluxes.

A. Neutrino fluxes

Following Kuo and Pantaleone [16], we denote the flux of various flavors of neutrinos and antineutrinos produced in

the core of the supernova by F_i^0, where i denotes all the flavors. In particular we use the generic label F_x^0 for flavors other than ν_e and $\overline{\nu_e}$ since

$$F_x^0 = F_{\nu_\mu}^0 = F_{\overline{\nu}_\mu}^0 = F_{\nu_\tau}^0 = F_{\overline{\nu}_\tau}^0. \tag{18}$$

All these flavors are produced via the neutral-current (NC) pair production processes and therefore have the same flux for all practical purposes. However, the ν_e and $\overline{\nu_e}$ fluxes are different from each other and the rest since they are produced not only by pair production but also derive a contribution from charged-current (CC) processes.

In the presence of matter, the flux emerging from the core undergoes changes due to oscillations as was discussed in the previous section. The flux reaching the detector from a supernova at a distance d from Earth is reduced by an overall geometric factor of $1/(4\pi d^2)$. Apart from this, there is a further modification of the observed flux due to oscillations. The flux on Earth, in the various flavors, is given in terms of the flux of neutrinos produced in the core of the supernova by

$$\begin{aligned} F_{\nu_e} &= P_{ee}F_{\nu_e}^0 + P_{e\mu}F_{\nu_\mu}^0 + P_{e\tau}F_{\nu_\tau}^0 \\ &= F_{\nu_e}^0 - (1-P_{ee})(F_{\nu_e}^0 - F_x^0), \end{aligned} \tag{19}$$

where we have made use of the constraint $\Sigma_j P_{ij} = 1$ and P_{ex} denotes the probability of a flavor μ or τ neutrino emerging as an electron neutrino. Since ν_μ- and ν_τ-induced events cannot be separated in water Cherenkov detectors, their combined flux on Earth may be written as

$$\begin{aligned} 2F_x &= F_{\nu_\mu} + F_{\nu_\tau} \\ &= 2F_x^0 + (1-P_{ee})(F_{\nu_e}^0 - F_x^0). \end{aligned} \tag{20}$$

Note that flavor mixing does not affect the total flux.

Similar expressions hold for antineutrino flavors with appropriate changes, that is,

$$F_{\overline{\nu}_e} = F_{\overline{\nu}_e}^0 - (1-\overline{P}_{ee})(F_{\overline{\nu}_e}^0 - F_x^0) \tag{21}$$

and

$$2F_{\overline{x}} = 2F_x^0 + (1-\overline{P}_{ee})(F_{\overline{\nu}_e}^0 - F_x^0). \tag{22}$$

Since $P_{ee} \neq \overline{P}_{ee}$, in general, the mixing breaks the equality of the ν_x and $\overline{\nu_x}$ fluxes.

We use the luminosity and average energy distributions (as functions of time) as given in Totani *et al.* [15], based on the numerical modelling of Mayle, Wilson, and Schramm [14]. The neutrino number flux is described, in a given time interval, Δt, as a thermal Fermi Dirac distribution

$$\frac{dF_i^0(j)}{dE} = N_0 \frac{\mathcal{L}_i}{T_j^4} \frac{E^2}{[\exp(E/T_j)+1]}, \tag{23}$$

for neutrinos of flavor j and energy E at a time t after the core bounce. Here i refers to the time bin, $t = t_0 + i\Delta t$. Hereafter, we set the time of bounce, $t_0 = 0$. The overall normalization N_0 is fixed by requiring that the total energy emitted per unit time equals the luminosity $\mathcal{L}_i$ in that time interval.

The thermal distribution that we have used (where the chemical potential has been set to zero) results in a flux that shows a slower fall with energy E than the results of the corresponding numerical model used in Ref. [15]; however, the effect of this on the event rates is small, of the order of a few percent. Typically, this distribution corresponds to an average neutrino energy or temperature ($\langle E_j \rangle \simeq 3.15 T_j$) of $\langle E(\nu_e) \rangle \sim 12$ MeV, $\langle E(\overline{\nu_e}) \rangle \sim 16$ MeV, and $\langle E(\nu_x) \rangle \sim 24$ MeV. Beyond about 1 s after the bounce, the average energies remain constant over the emission times of the supernova. However, the luminosities decrease, with very little emission beyond 10 s. Hence, in order to compute the event rates, we consider neutrino emission up to 10 s after bounce. The total emitted energy in all flavors of neutrinos up to this time is about 2.7×10^{53} ergs, which is more or less equally distributed in all flavors. The number of neutrinos emitted in each flavor, however, is not the same since their average energies are different.

B. Interaction at the detector

The basic quantity we are interested in is the distribution of events in the detector as a function of the energy of the detected particle. In the case of a water Cherenkov detector, this corresponds to the detection of a charged lepton in the final state. Here we are concerned with detection of electrons (or positrons) with energy, E_e. The various processes of interest therefore are the interactions of the neutrinos: (1) with electrons in water as targets,

$$\nu_l(\overline{\nu_l}) + e^- \rightarrow \nu_l(\overline{\nu_l}) + e^-, \quad l = e, \mu, \tau; \tag{24}$$

(2) with free protons in water as targets,

$$\overline{\nu_e} + p \rightarrow e^+ + n; \tag{25}$$

(3) with oxygen nuclei in water as targets,

$$\begin{aligned} \nu_e + {}^{16}\mathrm{O} &\rightarrow e^- + {}^{16}\mathrm{F}, \\ \overline{\nu_e} + {}^{16}\mathrm{O} &\rightarrow e^+ + {}^{16}\mathrm{N}. \end{aligned} \tag{26}$$

The cross sections $d\sigma/dE_e$ for all these processes, except the ones on oxygen, are well known [23,24]. The oxygen cross sections have been taken from Fig. 1 of Haxton [25]. As the interactions on protons and oxygen nuclei are purely CC interactions, they involve only ν_e and $\overline{\nu_e}$. Reaction (1) involves both CC and NC interactions for ν_e and $\overline{\nu_e}$ and only NC interactions for all other flavors.

The $\overline{\nu_e} p$ cross section is the largest, being proportional to the square of the antineutrino energy. In terms of the total number of events, therefore, water Cherenkov detectors are mostly dominated by $\overline{\nu_e}$ events. However, the different interactions in the detector have distinct angular signatures; this may be used to distinguish them. The elastic electron cross sections are forward peaked, especially for neutrinos with energies $\lesssim 10$ MeV [24,26], while the proton cross section is isotropic in the laboratory frame. Finally, the CC ν_e ($\overline{\nu_e}$)

cross section on oxygen, although having a rather large threshold of 15.4 MeV (11.4 MeV) [25], increases rapidly with incoming neutrino energy and is somewhat backward peaked. The higher the temperature at which the neutrino is emitted, the larger is this backward peak; hence it may be possible to distinguish this contribution from the rest by angular resolution as well, especially if there is substantial mixing between ν_e (or $\bar{\nu}_e$) and ν_x since the latter have a considerably hotter spectrum.

C. Event rates

The time-integrated event rate, from neutrinos of flavor j and energy E, as a function of the recoil electron (or positron) energy, is given by

$$\frac{dN^t(j)}{dE_e} = \frac{N_t}{4\pi d^2} \sum_i \int dE \frac{dF_i(j)}{dE} \frac{d\sigma_p}{dE_e}, \tag{27}$$

where the flux distribution $dF(j)/dE$ includes the effects of mixing in the hot dense core and the index t refers to any of the various processes through which the neutrino j can interact with the detector. Here N_t refers to the number of scattering targets (of either e, p, or ^{16}O) that are available in the detector. The total number of events from a given flavor of neutrino in a given bin k of electron energy (which we choose to be of width 1 MeV) then is the sum over all possible processes integrated over the bin width of the event rate:

$$N(j,k) = \sum_t \int_k^{k+1} dE_e \frac{dN^t(j)}{dE_e}. \tag{28}$$

In the next section, we shall use this formula to compute the time-integrated event rates for neutrino scattering with and without mixing, in water Cherenkov detectors, as a function of the detected electron (or positron) energy, in order to examine the effects of neutrino oscillations on supernova neutrino fluxes.

IV. RESULTS AND DISCUSSION

We compute the time-integrated event rate at a prototype 1 kton water Cherenkov detector from neutrinos emitted by a supernova exploding 10 kpc away. Results for any other supernova explosion may be obtained by scaling the event rate by the appropriate distance to the supernova and the size of the detector, as shown in Eq. (27). We assume the efficiency and resolution of such a detector to be perfect. Including these effects does not change the results by more than a few percent, as we will see. In fact, the maximum variation is at low energies, close to the threshold, where the low detector efficiency leads to lower detection rates.

The following constraints, derived from solar and atmospheric neutrino observations, are imposed. We begin with the constraints in the neutrino sector. Here, the angle ω does not play a role. As stated earlier, the (13) mixing angle is severely restricted: $\phi < 12°$. The solar and atmospheric neutrino problems allow for a wider choice in ϕ. This restriction on ϕ comes mainly from the CHOOZ experiment [27]. Since the survival probability P_{ee} depends only on this angle ($P_{ee} = \sin^2\phi$), this implies that $P_{ee} < 0.05$ and is thus very small. The observed dynamics of electron-type neutrinos, therefore, is completely driven by mu- and tau-type neutrinos produced in the supernova:

$$F_{\nu_e} \simeq F_x^0,$$

$$2F_x \simeq (F_x^0 + F_{\nu_e}^0). \tag{29}$$

Hence, as a result of mixing, the original electron neutrino flux is virtually replaced by the μ or τ neutrino flux. The cross sections at the detector increase with energy. Since the average energy of ν_x is of the order of $\sim$24 MeV while that of ν_e is $\sim$11 MeV, the effect of mixing and matter in the dense core is to dramatically increase the number of events due to e-type neutrinos while reducing the corresponding ν_x contribution.

We now discuss the antineutrino sector. While the same limits apply on ϕ, we now have to consider the limits on the (12) mixing angle ω as well. The constraints on ω mainly emerge from the solar neutrino problem. (For a recent review, see Ref. [30].) The best global Mikheyev-Smirnov-Wolfenstein (MSW) fit gives $\delta_{12} \sim 10^{-6}$ eV^2 and $\sin^2 2\omega = 5.5 \times 10^{-3}$. There is also a large angle solution with MSW fit. For vacuum oscillations, the fit gives $\delta_{12} \sim 10^{-10}$ eV^2 and $\sin^2 2\omega = 0.75$. In the present analysis, $\delta_{12} < 10^{-4}$ eV^2, which is consistent with both MSW and vacuum solutions. For ω, therefore, we choose two possible values, viz., ω small and ω large. These two typical choices cover the extreme ends of the possible effects of mixing in supernova neutrinos.

If ω is small (corresponding to the MSW solution to the solar neutrino problem), then the antineutrino survival probability becomes, $\bar{P}_{ee} = \cos^2\phi \cos^2\omega \to \cos^2\phi \to 1$, since ϕ is small. This, in effect, is similar to the no-mixing solution. The large angle solution allows for a near-maximal mixing of $\omega \sim 45°$; in this case, the survival probability becomes $\bar{P}_{ee} = \cos^2\phi \cos^2\omega \to 1/2$ and this corresponds to maximal mixing in the antineutrino sector. Therefore we have

$$F_{\bar{\nu}_e} \simeq \frac{1}{2}(F_{\bar{\nu}_e}^0 + F_x^0),$$

$$2F_{\bar{x}} \simeq \frac{1}{2}(3F_x^0 + F_{\bar{\nu}_e}^0). \tag{30}$$

In any case, we have the result that $\bar{P}_{ee} \lesssim 0.5$ for any choice of ω when ϕ is small. Hence, typically, the antineutrino fluxes that reach the Earth are combinations of $\bar{\nu}_e$ and $\bar{\nu}_x$ fluxes. Again, since the average energies of $\bar{\nu}_e$ and $\bar{\nu}_x$ are 15 and 24 MeV, respectively, this results in an enhanced $\bar{\nu}_e$ event rate and a reduced $\bar{\nu}_x$ rate at the detector. It is important to note that these flux mixings are energy independent. For example, the energy spectrum of a given neutrino flavor produced in the supernova is not altered during propagation; however, its flavor content at the detector will depend on the

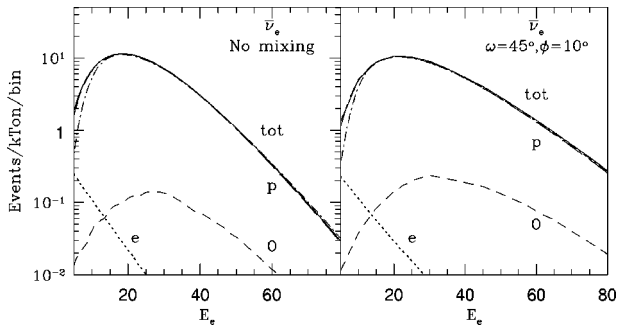

FIG. 1. The number of events in bins of electron energy of 1 MeV each, due to $\overline{\nu}_e$ interactions, is shown as a function of the electron energy, with and without mixing. The long-dashed, dashed, and dotted lines correspond to interactions with *p*, *O*, and *e*, respectively, in the detector. The dot-dashed line indicates the effect of inclusion of detector efficiency and resolution on the interaction with *p*. See the text for more details. The solid line denotes the total contribution to the event rate from $\overline{\nu}_e$.

extent of mixing. We shall now probe the quantitative effects of these mixings on the observed event rates.

We first consider the case where there is no neutrino mixing. The largest contribution comes from the $\overline{\nu}_e p$ interaction, which has a cross section proportional to the square of the antineutrino energy. This is shown in the left-hand part of Fig. 1, where the number of events, $N(k)$, in the kth bin is plotted against the central values of the recoil electron energy in that bin. In comparison, the $\overline{\nu}_e e$ contribution is negligibly small. However, this is not the case with the $\overline{\nu}_e O$ contribution, which, though small, may be measurable at, say, the large (32 kton) SuperKamiokande detector. It can be seen, though, that the total rate is saturated by the proton interaction. Neutrino mixing causes an increase in the high energy event rates, as can be seen from the right-hand side of Fig. 1. Here, we have used typical values for $\omega(=45°)$ and $\phi(=10°)$; this choice of ω maximizes mixing effects. The other (small-angle) solution for ω is similar to the no-oscillation scenario shown on the left-hand side of the figure. Note that our three-flavor analysis precludes the choice $\omega,\phi=0$. For example, the result that ν_e starts out as a pure ν_3 mass eigenstate in the stellar core will not hold if $\phi=0$.

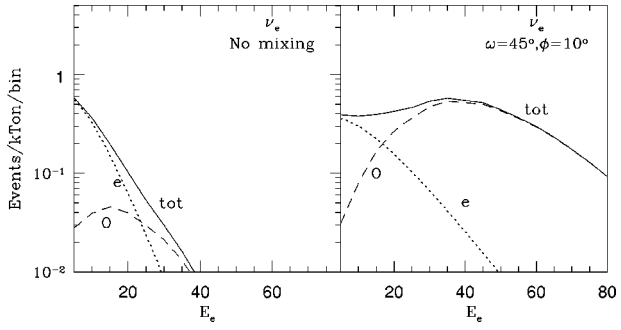

FIG. 2. The number of events in bins of 1 MeV each, due to ν_e interactions, is shown as a function of the electron energy, with and without mixing. The dashed and dotted lines correspond to interactions with *O* and *e*, respectively, in the detector. The solid line denotes the total contribution to the event rate from ν_e.

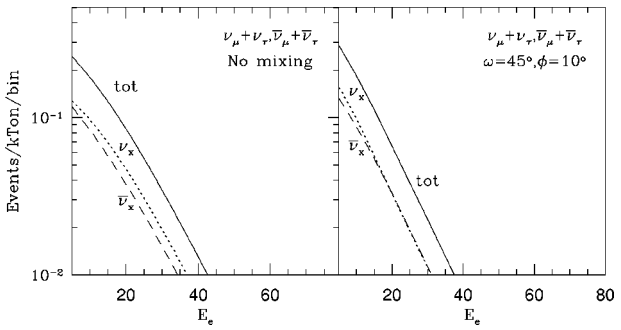

FIG. 3. The number of events in bins of 1 MeV each, with and without mixing, due to $\nu_{\mu,\tau}e$ and $\overline{\nu}_{\mu,\tau}e$ elastic scattering in the detector, is shown as a function of the electron energy, as dotted and dashed lines, respectively. The solid line denotes the total contribution to the event rate from all these channels, that is, from ν_μ, ν_τ, $\overline{\nu}_\mu$, and $\overline{\nu}_\tau$.

The corresponding results for ν_e events are shown in Fig. 2. While the no-mixing contributions are negligible, it is seen that there is a more than tenfold increase in the event rate due to scattering off oxygen. The low no-mixing rate was because the average ν_e energy is less than the threshold energy required for this reaction to proceed. Mixing opens up this channel since there are now many more ν_e, originating as ν_x in the star, which are more energetic. Since the backward peak in the $\nu_e O$ cross section is more pronounced for flux distributions at higher temperatures [25], it may be possible to separate these events from the bulk of the antielectron neutrino events at the detector.

Finally, we see from Fig. 3 that there is a low-energy enhancement of the ν_x and $\overline{\nu}_x$ rates upon mixing. Their contribution, however, is still small, of the order of the $\nu_e e$ elastic scattering events. For comparison, all the contributions, with and without mixing, are shown in Fig. 4. It is clear that the proton absorption events are the largest, independent of mixing. However, it is the $\nu_e O$ events which are most sensitive to the amount of mixing, and are likely to be most important in furthering our understanding of neutrino oscillations in vacuum and matter.

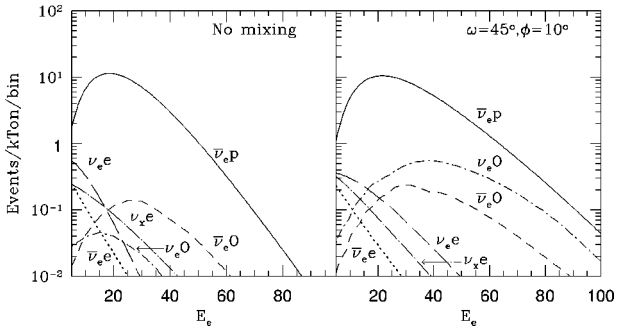

FIG. 4. A comparison of the number of events in bins of 1 MeV each, due to various processes, is shown as a function of the electron energy, with and without mixing. The line types indicate events from the processes $\overline{\nu}_e p$ (solid line), $\overline{\nu}_e e$ (dotted line), $\overline{\nu}_e O$ (dashed line), $\nu_e e$ (long-dashed line), $\nu_e O$ (dot-dashed line), and $\nu_x e$ (dot-long dashed line) processes, respectively. The subscript x denotes the NC contribution from ν_μ, ν_τ, and their antiparticles.

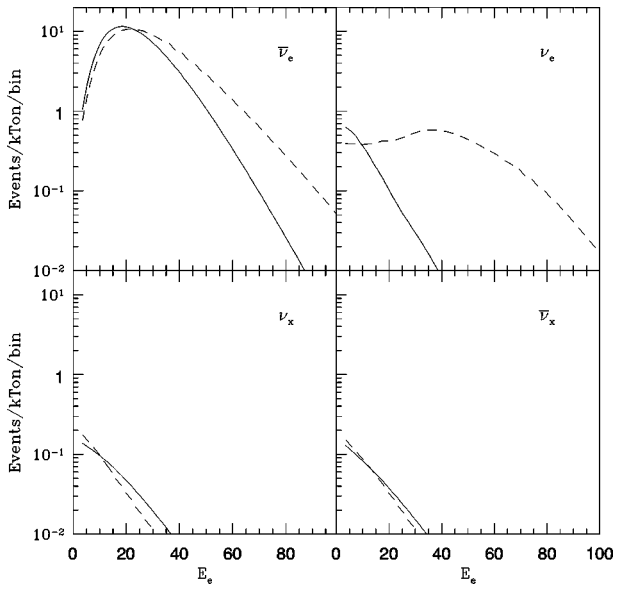

FIG. 5. The total number of events (summed over all processes) in bins of 1 MeV each, due to $\bar{\nu}_e$, ν_e, $\nu_{\mu,\tau}$, and $\bar{\nu}_{\mu,\tau}$ interactions, is shown as a function of the electron energy. The solid and dashed lines denote the event rates without and with (maximal effect due to) mixing.

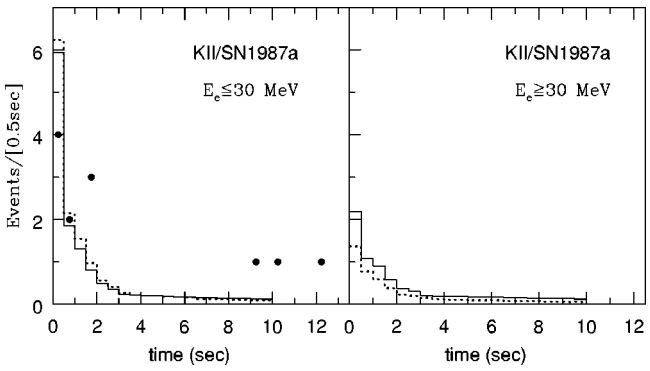

FIG. 6. The time-dependent neutrino spectrum (due to $\bar{\nu}_e p$ scattering) in bins of 0.5 s is shown as a function of the time of detection, in comparison with the events observed at the Kamiokande II detector from the supernova SN 1987a. The dashed and solid lines correspond to the number of events without and with (maximal effect due to) mixing. The low- and high-energy components of the signal are separately shown.

We recall that the proton absorption events are isotropic and the scattering off oxygen is backward enhanced, while the elastic scattering on electrons is mostly forward peaked. In fact, even the elastic ν_e and ν_x (including antineutrinos) events may be separated based on angular resolution [26]. Hence, it is likely that a nearby supernova explosion (at a distance of about 10 kpc, say) can yield information *independently* on the various neutrino flavors, ν_e, $\bar{\nu}_e$, and ν_x. We have therefore shown the total contribution from each of these flavors, with and without neutrino mixing, in Fig. 5. For a 32 kton detector such as SuperKamiokande, this translates to a total event rate of 12 235 events with mixing as opposed to 9871 events without mixing, a 25% increase, with individual channels contributing as shown in Table I. Note that the thermal flux distribution, while agreeing with the numerical model of Ref. [15] at lower energies, overestimates the flux at larger energies. Hence, the number of events at high energies may be overestimated in this model. However, we emphasize that the *relative* increase, with and without oscillation, remains the same.

We now briefly discuss these results in relation to the supernova SN 1987A. Recall that the supernova, which was 55 kpc away, was detected by KII, which was a 2.14 kton (fiducial volume) water Cherenkov detector; the corresponding results for this can therefore be obtained from our analysis by multiplying the results by a factor of 2.14/30.25. However, since KII mostly detected low-energy events, we have now included the detector efficiency [17] in our analysis. The event rate is determined entirely by the $\bar{\nu}_e p$ events. Since KII measured the time dependence of the spectrum, we have shown our results for the event rate as a function of time in Fig. 6. The figure on the left-hand side of Fig. 6 shows the event rates for energies from $8<E_e(\mathrm{MeV})<30$ MeV, which is the energy range in which KII made observations; the dotted curve indicates the contribution in

TABLE I. Event rates with and without oscillation for a supernova explosion at a distance of 10 kpc. The high-energy events, which are given separately, show the enormous enhancement in the *p* and *O* channels, with oscillation. Results are shown for a 1 kton water Cherenkov as well as for the 32 kton (fiducial volume) SuperKamiokande detectors.

Detector	$\nu_e e$	$\nu_e O$	$\bar{\nu}_e e$	$\bar{\nu}_e O$	$\bar{\nu}_e p$	$\nu_{\mu,\tau} e$	$\bar{\nu}_{\mu,\tau} e$
				$E_e>8$ MeV			
1 kton (no osc)	2.3	1.0	0.8	3.8	272.0	1.3	1.0
1 kton (max osc)	4.2	23.8	0.9	8.1	323.2	1.0	1.0
SuperK (no osc)	72.4	30.8	25.1	123.0	8702.9	41.1	33.4
SuperK (max osc)	134.6	761.0	30.0	260.6	10343.9	31.5	31.7
				$E_e>30$ MeV			
1 kton (no osc)	0.0	0.2	0.0	1.8	76.6	0.2	0.2
1 kton (max osc)	0.7	18.4	0.1	5.4	138.6	0.1	0.1
SuperK (no osc)	1.5	5.9	1.0	56.2	2450.0	6.4	4.9
SuperK (max osc)	22.2	587.6	2.2	172.8	4436.5	3.5	4.1

the absence of mixing. It is seen that mixing marginally decreases the event rate while it almost doubles the rate for events with energies $E_e > 30$ MeV as can be seen from the figure on the right. This separation has been done since the thermal Fermi-Dirac distribution that we use overestimates the flux at larger (neutrino) energies due to a very large high-energy tail compared to the corresponding numerical model [15], while agreeing quite well at lower energies $E_{\bar{\nu}_e} \sim E_e < 30$ MeV. This is particularly true for the event rate at early times; hence our high-energy predictions may be overestimated by a factor of 4 or more. Note, however, that even if the absolute spectrum is overestimated by the model we have used, the results we had shown earlier contrast the relative differences with and without mixing and still hold. Finally, the model also predicts that high-energy events are most likely to occur at early times in the supernova explosion. This is not inconsistent with the observations of KII [2].

To summarize, a great deal of the physics of neutrino mixing and the effects of dense matter in neutrino propagation may be tested from neutrinos emitted during supernova explosions. Specifically, from the results summarized in Table I, we may conclude the following.

(1) The observed $\bar{\nu}_e p$ events are the largest in number as well as least sensitive to the mixing parameters. Hence they provide a direct test of the supernova models. Since the angular distribution of these events is isotropic, they may be used to set the overall normalization.

(2) All the interactions involving electrons as targets are peaked in the forward direction (in fact, for $E_\nu > 8$ MeV, more than 90% of them lie in a 10° cone with respect to the supernova direction). In the absence of any mixing, there will also be a few events in the backward direction due to CC scattering on oxygen targets. As indicated in Table I, the forward-backward asymmetry in the event distribution will be clearly marked.

(3) The main effect of mixing is then to produce a dramatic increase in the events involving oxygen targets. As remarked earlier, this will show up as a marked increase in the number of events in the backward direction with respect to the forward-peaked events. The actual increase, however, will depend sensitively on a combination of both the mixing parameters as well as the supernova model.

We have limited our analysis in this paper to a model with three active neutrino generations and possible mixings among them. This allows us to incorporate constraints arising from solar and atmospheric neutrino problems. This, however, leaves out a new set of constraints which may emerge from the results of the LSND experiments [31]. The LSND results cannot be accommodated within the three-generation formalism, with the parameter ranges used in our analysis. One may therefore require a sterile neutrino with a new mass scale, leading to yet another mass-squared difference $\delta \sim 0.3$–$1\ \mathrm{eV}^2$ [32]. In the context of supernova neutrinos, this opens up yet another channel for $\nu_{\mu,\tau}$ to oscillate and may therefore reduce the dramatic enhancement one sees in the ν_e events.

Note added in proof. After this paper was submitted, we came across a paper by Fuller, Haxton, and McLaughlin [33] in which the importance of electron-neutrino and electron-antineutrino events on oxygen in determining the effect of mixing has been pointed out. Also, the assumption made in this paper, and almost all the others, that the $\bar{\nu}_e p \to e^+ n$ process is isotropic is correct only to the leading order. The corrections due to weak magnetism not only reduce the cross section by a few percent, but also render the positron distribution to be not isotropic, although the effect is small. In fact, the positrons are slightly backward peaked below 15 MeV, whereas they are slightly forward peaked above this energy (see Vogel and Beacom [33]). These corrections have, however, negligible impact on the energy spectrum and the total event rate. We are grateful to John Beacom for pointing out these facts.

ACKNOWLEDGMENTS

We thank Kamales Kar for many useful discussions and a critical reading of the paper.

APPENDIX A

The time evolution of the neutrino mass eigenstates in vacuum is given by

$$\nu_i(t) = \exp[-iE_i t]\nu_i(0), \quad i = 1,2,3.$$

Assuming the neutrino masses to be small, in the extreme relativistic limit, we have

$$E_i \simeq p + \frac{\mu_i^2}{2p},$$

where μ_i $(i=1,2,3)$ denotes the neutrino masses. In the presence of matter, neutrinos interact with electrons, protons, and neutrons in matter. While ν_e $(\bar{\nu}_e)$ interact both via CC and NC interactions, ν_x $(\bar{\nu}_x)$ scatters via NC interactions alone. Note that the interaction with matter is diagonal in the flavor basis but not in the mass basis. As a result, the dispersion relation in matter is given by

$$E_i \simeq p + \frac{m_i^2}{2p},$$

where m_i are now eigenvalues of the $(\mathrm{mass})^2$ matrix given by

$$M_m^2 = M_\nu^2 + M_{\mathrm{int}}^2.$$

Here the mass-squared matrix in vacuum, M_ν^2, is defined in Eqs. (3) and (4) and M_{int} is given by

$$M_{\mathrm{int}}^2 = \pm\sqrt{2}G_F p[-\{(1-4\sin^2\theta_W)(N_e - N_p) + N_n\}II + 2N_e M_A].$$

Here N_e, N_p, and N_n denote the number densities of electrons, protons, and neutrons in matter, M_A is the matrix defined in Eq. (7) of Sec. II, and θ_W is the Weinberg angle. Note that $(1-4\sin^2\theta_W)$ is close to zero and that the matrix M_{int}^2 is expressed in the flavor basis. The upper sign corre-

sponds to neutrinos (ν_e, ν_μ, and ν_τ) while the lower sign corresponds to antineutrinos ($\bar{\nu}_e$, $\bar{\nu}_\mu$, and $\bar{\nu}_\tau$).

We will now compute the eigenvalues m_i^2 in matter, ignoring the terms proportional to the unit matrix II, since we will only be interested in differences between the eigenvalues. Consider the eigenvalues of the matrix defined by

$$\Delta M_m^2 \equiv A(r) M_A + \delta_{31} M_{31} + \delta_{21} M_{21},$$

where $\delta_{ij} = \mu_i^2 - \mu_j^2$ and M_{31}, M_{21} are matrices defined in Eq. (5) and $A(r)$, the matter-dependent (and hence distance dependent) term, $A(r) = \pm 2\sqrt{2} G_F N_e E$ for ν_e and $\bar{\nu}_e$, respectively, varies linearly with the matter density. Since neutrinos are produced in the high-density region of the supernova, $|A(\text{core})| \simeq 2 \times 10^7 E$ eV^2, where E is the neutrino energy in MeV. Thus $|A(\text{core})| \gg \delta_{31} \gg \delta_{21}$.

We now compute the eigenvalues perturbatively. Since δ_{31} and δ_{21} are different from each other, the resonances, if they occur, are well separated. We therefore diagonalize the first two terms in ΔM_m^2 and treat the third term as a perturbation. The eigenvalues are then given by

$$\delta m_1^2 = \frac{A + \delta_{31}}{2} + \frac{1}{2}[(A - \delta_{31}\cos 2\phi)^2 + (\delta_{31}\sin 2\phi)^2]^{1/2} + \delta_{21}\cos^2(\phi - \phi_m)\sin^2\omega, \tag{A1}$$

$$\delta m_2^2 = \delta_{21}\cos^2\omega, \tag{A2}$$

$$\delta m_3^2 = \frac{A + \delta_{31}}{2} - \frac{1}{2}[(A - \delta_{31}\cos 2\phi)^2 + (\delta_{31}\sin 2\phi)^2]^{1/2} + \delta_{21}\sin^2(\phi - \phi_m)\sin^2\omega, \tag{A3}$$

where the matter mixing angles are given by

$$\tan 2\phi_m = \frac{\delta_{31}\sin 2\phi}{\delta_{31}\cos 2\phi - A}$$

and

$$\tan\omega_m = \mathcal{O}\left(\frac{\delta_{21}}{A}\right).$$

To the leading order, the mixing matrix in matter, $U_m(\phi_m, \omega_m)$, is given by

$$U_m = \begin{bmatrix} c_{\phi_m} & \Lambda s_{\phi_m} & s_{\phi_m} \\ 0 & 1 & -\Lambda \\ -s_{\phi_m} & \Lambda c_{\phi_m} & c_{\phi_m} \end{bmatrix},$$

which is unitary, up to $\mathcal{O}((\delta_{21}/\delta_{31})^2)$. Here c and s stand for cos and sin, respectively; for example, c_{ϕ_m} denotes $\cos\phi_m$; $\Lambda = (\delta_{21}/\delta_{31}) s_{(\phi - \phi_m)} s_\omega c_\omega$. Terms of order $\mathcal{O}(\delta_{21}/A)$ are neglected in U_m.

Up until now, the only approximation that has been used is the hierarchy $A \gg \delta_{31} \gg \delta_{21}$. Using this hierarchy and the value of $A(\text{core})$ given earlier, we find

$$\phi_m \rightarrow \begin{cases} \pi/2 & \text{for neutrinos,} \\ 0 & \text{for antineutrinos.} \end{cases}$$

This result, when combined with the definition of the matter mixing matrix U_m, leads to the fact that ν_e's are produced almost entirely in the $|\nu_3\rangle$ mass eigenstate whereas $\bar{\nu}_e$ are produced almost entirely in the mass eigenstate $|\bar{\nu}_1\rangle$ in the dense stellar core.

If the propagation is adiabatic, this also implies that the averaged survival probability of electron neutrinos is given by

$$P_{ee} = |\langle \nu_e(t) | \nu_3(0)\rangle|^2 = s_\phi^2,$$

and that of the antielectron neutrino is given by

$$\bar{P}_{ee} = |\langle \bar{\nu}_e(t) | \bar{\nu}_1(0)\rangle|^2 = c_\phi^2 c_\omega^2,$$

where t denotes the time of detection of the neutrino on Earth.

In Appendix B we show that the propagation is indeed adiabatic and the expressions given above provide a reasonably accurate description of the matter effects in the stellar interior.

A few remarks about the eigenvalues δm_i^2 are in order. Note that the eigenvalues themselves are always positive definite for electron-type neutrinos, whereas for muon-type neutrinos or electron antineutrinos, this is not always the case since A is large and negative. The complete dispersion relation for the energy eigenvalues is given by

$$E_i \simeq p + \frac{1}{2p}[\mu_i^2 \mp \sqrt{2} G_F p\{(1 - 4\sin^2\theta_W)(N_e - N_p) + N_n\} + \delta m_i^2].$$

The effect of the CC interactions with matter gives rise to the δm_i^2 term. The NC term, common to all flavors, is now included here. The second term in the expression for E_i is typically of the order of tens of eV in the stellar core. Therefore, for energies $E \sim p \sim$ few MeV, the second term is small and may be neglected except when computing matter mixing angles. However, for neutrinos having energies of the order of tens of eV (but still with $p \gg \mu_i$), the two terms compete. Since the sign of the second term changes depending on whether the particle scattering is a neutrino or an antineutrino, one may expect interesting phenomena when E_i becomes negative. This may lead to the trapping of low-energy neutrinos. This phenomenon is unique to neutrinos produced in supernova explosions. While it is of little relevance to the detection of neutrinos on Earth, it may have interesting astrophysical consequences. The dynamics of such neutrinos is under further investigation.

APPENDIX B

The electron neutrino ν_e is produced in the core of the supernova in the mass eigenstate $|\nu_3\rangle$ with a negligible admixture of the other two states. As the produced $|\nu_3\rangle$ propa-

gates outwards, it passes through variable density matter (since the density inside the stellar core decreases monotonically outwards). Such a propagation may in general induce the presence of other mass eigenstates (since they are no longer eigenstates of the Hamiltonian) by the time the neutrino exits the star and reaches the detector. The Landau-Zener ''jump probability'' or level transition probability [29] is maximal at the resonances and is given by

$$P_{LZ}=\exp\left[-\frac{\pi}{2}\gamma F\right],$$

where F is a factor which depends on the density profile and γ is the nonadiabaticity parameter.

Since ν_e is produced in the mass eigenstate $|\nu_3\rangle$, we first consider the crossover between $|\nu_3\rangle$ and $|\nu_2\rangle$. Then,

$$\gamma=\frac{\delta\sin^2 2\phi}{2E\cos 2\phi\left|\frac{1}{N_e}\frac{dN_e}{dx}\right|_0},$$

where ϕ is the relevant mixing angle for the upper resonance and $\delta\equiv(\delta_{31}+\delta_{32}+\delta_{12}\cos 2\omega)/2\sim\delta_{31}$, independent of $\cos 2\omega$ [16], because of the assumption $\delta_{12}\ll\delta_{31}\sim\delta_{32}$. The suffix 0 indicates that the derivative in the density, N_e, is to be evaluated at resonance, when the eigenstates $|\nu_2\rangle$ and $|\nu_3\rangle$ are the closest.

The density profile in the core may be assumed to be of the form [16]

$$\rho(r)\sim\frac{C}{r^3},$$

where $1<C/10^{31}$ gm<15. (This assumption is not crucial but is sufficient for our analysis.) As a result, the nonadiabaticity parameter evaluates to

$$\gamma=\frac{R_0\delta_{31}}{6E}\left(\frac{\sin^2 2\phi}{\cos 2\phi}\right),$$

where R_0 is the radius at which the higher resonance occurs, i.e., when $A(r)\simeq\delta_{31}\cos 2\phi$. Using the explicit expression for $A(r)$, the resonant density is given by

$$\rho_0(\mathrm{g/cm^3})=\frac{6.6\times 10^5}{Y_e}\left(\frac{\delta_{31}}{e}\right)\cos 2\phi,$$

where δ_{31} is in eV^2 and $e=E/(10$ MeV$)$. Here $Y_e=Z/A\sim 0.5$ is the electron fraction in the matter. For $\delta_{31}\simeq 10^{-3}$ eV^2, as preferred by solar and atmospheric neutrino data, and a typical detected neutrino energy of 10 MeV, the resonant density is $\rho_0=1320(\cos 2\phi)$ g/cm^3. This determines the resonant radius R_0 for a given value of ϕ. If the angle ϕ is indeed small, as indicated by CHOOZ [27], this implies

$$R_0=\left(\frac{eC}{1320\times 10^{15}}\right)^{1/3}\ \mathrm{km},$$

which evaluates to 20 000–50 000 km for $E=10$ MeV ($e=1$).

The nonadiabaticity parameter is then given by (for R_0 in km),

$$\gamma\simeq\frac{5076R_0}{e}\left(\frac{\sin^2 2\phi}{\cos 2\phi}\right).$$

Since R_0 is large, it is clear that γ is large unless ϕ is very small. Furthermore, for small values of ϕ, $F\simeq 1$. In fact, for $\sin\phi\geqslant 10^{-2}$, we find $\gamma\gg 1$ so that the Landau-Zener probability is vanishingly small: $P_{LZ}<10^{-2}$. Our three-flavor analysis of the neutrino mixing problem in any case precludes the choice of $\phi=0$. Therefore, for all practical purposes, we assume $\phi>10^{-2}$ and hence consider the neutrino propagation in matter to be purely adiabatic. This implies that the $|\nu_e\rangle$ which is produced as $|\nu_3\rangle$ essentially remains in this mass eigenstate until it reaches the detector. For $\overline{\nu_e}$, which are produced mainly in the $|\overline{\nu_1}\rangle$ mass eigenstate, there is no resonance condition to be satisfied (the sign of A changes from neutrino to antineutrino) and hence the propagation is always adiabatic.

[1] IAU Circular No. 4316, 1987.

[2] Kamiokande II Collaboration, K. Hirata *et al.*, Phys. Rev. Lett. **58**, 1490 (1987).

[3] IMB Collaboration, R. M. Bionta *et al.*, Phys. Rev. Lett. **58**, 1494 (1987).

[4] N. D. Hari Dass, D. Indumathi, A. S. Joshipura, and M. V. N. Murthy, Curr. Sci. **56**, 575 (1987).

[5] J. Arafune and M. Fukugita, Phys. Rev. Lett. **59**, 367 (1987).

[6] J. N. Bahcall and S. N. Glashow, Nature (London) **326**, 476 (1987).

[7] K. Sato and H. Suzuki, Phys. Rev. Lett. **58**, 2722 (1987).

[8] W. D. Arnett and J. L. Rosner, Phys. Rev. Lett. **58**, 1906 (1987).

[9] E. Kolb, H. Stebbins, and M. Turner, Phys. Rev. D **35**, 3598 (1987).

[10] R. Cowsik, Phys. Rev. D **37**, 1685 (1988).

[11] For a recent review of the status of solar and atmospheric neutrinos, see, for example, P. Langacker, Nucl. Phys. B (Proc. Suppl.) **77**, 241 (1999).

[12] Mohan Narayan, G. Rajasekaran, and S. Uma Sankar, Phys. Rev. D **56**, 437 (1997); Mohan Narayan, M. V. N. Murthy, G. Rajasekaran, and S. Uma Sankar, *ibid.* **53**, 2809 (1996).

[13] G. L. Fogli, E. Lisi, A. Marrone, and G. Scioscia, Phys. Rev. D **59**, 117303 (1999); **59**, 033001 (1999); G. L. Fogli, E. Lisi, and D. Montanino, Astropart. Phys. **9**, 119 (1998); G. L. Fogli, E. Lisi, D. Montanino, and G. Scioscia, Phys. Rev. D **56**, 4365 (1997).

[14] A. Burrows and J.M. Lattimer, Astrophys. J. **307**, 178 (1986); R. Mayle, J. R. Wilson, and D. N. Schramm, *ibid.* **318**, 288 (1987).

[15] T. Totani, K. Sato, H. E. Dalhed, and J. R. Wilson, Astrophys. J. **496**, 216 (1998); see also the references in [14] above.

[16] T. K. Kuo and J. Pantaleone, Phys. Rev. D **37**, 298 (1988).
[17] Y-Z. Qian and G. M. Fuller, Phys. Rev. D **49**, 1762 (1994).
[18] Sandhya Choubey, Debasish Majumdar, and Kamales Kar, J. Phys. G **25**, 1001 (1999).
[19] J. F. Beacom and P. Vogel, Phys. Rev. D **58**, 053010 (1998); **58**, 093012 (1998).
[20] Sandhya Choubey and Kamales Kar, hep-ph/9905327.
[21] T. K. Kuo and J. Pantaleone, Phys. Rev. D **35**, 3432 (1987).
[22] A. S. Joshipura and M. V. N. Murthy, Phys. Rev. D **37**, 1374 (1988).
[23] G. 't Hooft, Phys. Lett. **37B**, 195 (1971).
[24] J. N. Bahcall, *Neutrino Astrophysics* (Cambridge University Press, Cambridge, England, 1989).
[25] W. C. Haxton, Phys. Rev. D **36**, 2283 (1987).
[26] A. de Gouvêa and H. Murayama, Phys. Rev. Lett. **82**, 3392 (1999).
[27] CHOOZ Collaboration, M. Apollonio *et al.*, Phys. Lett. B **420**, 397 (1998).
[28] Mohan Narayan, G. Rajasekaran, and S. Uma Sankar, Phys. Rev. D **58**, 031301 (1998).
[29] See, for example, S. J. Parke, Phys. Rev. Lett. **57**, 1275 (1986).
[30] J. N. Bahcall, P. I. Krastev, and A. Yu. Smirnov, Phys. Rev. D **58**, 096016 (1998).
[31] LSND Collaboration, C. Athanassopoulos, Phys. Rev. Lett. **81**, 1774 (1998).
[32] For a recent review, see J. W. F. Valle, invited talk at the Ioannina Conference, ''Symmetries in intermediate and high energy physics and its applications,'' hep-ph/9906378, 1998.
[33] G. M. Fuller, W. C. Haxton, and G. C. McLaughlin, Phys. Rev. D **59**, 085005 (1999); P. Vogel and J. F. Beacom, *ibid.* **60**, 053003 (1999).